



First science with SPHERE

R. Claudi¹, R. Gratton¹, S. Desidera¹, A.-L. Maire¹, D. Mesa¹, M. Turatto¹,
A. Baruffolo¹, E. Cascone², V. De Caprio¹, V. D’Orazi¹, D. Fantinel¹, E. Giro¹,
B. Salasnich¹, S. Scuderi³, E. Sissa¹, J.-L. Beuzit⁴, and D. Mouillet⁴

¹ INAF – Osservatorio Astronomico di Padova, Vicolo Osservatorio,5 I-35122 Padova, Italy, e-mail: riccardo.claudi@oapd.inaf.it

² INAF – Osservatorio Astronomico di Capodimonte, Via Moiariello,16 I-80131 Napoli, Italy

³ INAF – Osservatorio Astrofisico di Catania, Via di S. Sofia,78 I-95123 Catania, Italy

⁴ Institut de Planétologie et d’Astrophysique de Grenoble, B.P. 53, F-38041 Grenoble Cedex 9, France

Abstract. The Spectro-Polarimetric High-contrast Exoplanet Research (SPHERE) facility mounted at ESO-VLT aims at discovering giant extrasolar planets in the proximity of bright stars and characterising them through spectroscopic and polarimetric observations. SPHERE is a complete system with a core made of an extreme-Adaptive Optics (XAO) turbulence correction, a pupil tracker and NIR and Visible coronagraph devices. At its back end, a differential dual imaging camera (IRDIS) and an integral field spectrograph (IFS) work in the Near Infrared (NIR) ($0.95 \leq \lambda \leq 2.32 \mu\text{m}$) while a high resolution polarization camera covers the visible domain ($0.6 \leq \lambda \leq 0.9 \mu\text{m}$). The IFS is a low resolution spectrograph ($R \sim 50$) that operates in the near IR ($0.95 \leq \lambda \leq 1.6 \mu\text{m}$), an optimal wavelength range for the detection of planetary features, over a field of view of about 1.7×1.7 square arcsecs. From spectra it is possible to reconstruct monochromatic images with high contrast (10^{-6} at 0.5 arcsec) and high spatial resolution, well inside the star PSF. The commissioning of the instrument ended in October 2014 and ESO has already offered SPHERE to the community. In this paper several results obtained during the commissioning and science verification phase are described.

Key words. Extrasolar Planets – High Contrast Imaging – Direct Imaging

1. Introduction

In the skyline of the exoplanet discovery methods, direct imaging is the only one that allows to detect photons coming directly from the planet. The most productive methods in detection (radial velocity and transit methods) are both indirect methods and both suffer from bias effects due mainly to the star ac-

tivity signal. Direct imaging is not affected by these effects. For the time being direct imaging can observe low mass companions (BDs and Planets) in wide orbits or young planet in closer orbits with an inner limit of about 10 AU. In this context direct imaging is unique in probing the properties of the outer regions of planetary systems, having also the possi-

bility to study young systems (it is not sensitive to activity), the dynamical evolution of planetary systems and the connection between recently formed planets and the circumstellar environment. Furthermore direct imaging enables spectroscopy of non strongly irradiated giant planets opening the way to their physical characterisation. During the last few years, direct imaging of exoplanets from the ground has provided breakthrough results thanks to the commissioning of new-generation instruments. The SEEDS survey conducted with HiCIAO (Tamura et al. 2010) on the Subaru telescope allowed the detection of two planetary-mass companions to κ And (Carson et al. 2013) and GJ 504 (Kuzuhara et al. 2013). For the latter, strong absorptions of methane were revealed (Janson et al. 2013). Data analyses on the first years of this 5-year survey (120 nights) were published (Janson et al. 2013; Brandt et al. 2014a,b), which suggest that massive planets in debris disks similar to β Pictoris b (Lagrange et al. 2010) are rare and that the majority of the imaged planetary-mass companions formed in the same way as brown dwarfs. Project 1640 (Oppenheimer et al. 2012) at Palomar Observatory started a survey of 99 nights over 3 years in late 2012, and obtained near-infrared ($\sim 1 - 2 \mu m$) photometric and spectroscopic measurements of young brown dwarfs and giant planets (Oppenheimer et al. 2013; Hinkley et al. 2013). The adaptive optics facility of the Large Binocular Telescope (Esposito et al. 2012) and the LMIRCam instrument (Skrutskie et al. 2010) are employed for a survey of ~ 100 nights, which started in 2013 for a duration of 3–4 years (Skemer et al. 2014a) and allowed multi-wavelength photometry in the L band (Skemer et al. 2012, 2014b) ($3 - 4 \mu m$) of the four planets of HR 8799 (Marois et al. 2008, 2010) and M-band photometry of κ And b (Bonnefoy et al. 2014). The MagAO system on the Magellan telescope was commissioned late 2012 (Close et al. 2014). This instrument feeds two science cameras, VisAO in the visible and Clio2 in the near-infrared. A planetary-mass companion to HD106906 was detected with the near-infrared camera (Bailey et al. 2014). Visible observations allowed the confirmation of the low-

mass stellar companion discovered by Biller et al. (2012) in the gap of the transitional disk of HD 142527 (Close et al. 2013) and provided the first ground-based image in the visible ($\lambda \leq 0.985 \mu m$) of an exoplanet (Males et al. 2014). A survey to search for giant accreting protoplanets in the gaps of transitional disks has recently started (Close et al. 2013). The Gemini Planet Imager (GPI) saw its first light at the Gemini South telescope in November 2013 and achieved H-band Strehl ratios of 0.9 and 5σ contrasts of $10^{-5} - 10^{-6}$ at separations of 0.35-0.75 arcsec (Macintosh et al. 2014). Data analyses of commissioning observations of β Pictoris b (Lagrange et al. 2010) and HD 95086 b (Macintosh et al. 2014; Meshkat et al. 2013; Rameau et al. 2013) were published (Macintosh et al. 2014; Galicher et al. 2014). Finally, after crossing the ocean in February 2014, SPHERE (Beuzit et al. 2008) was reintegrated and tested at Paranal and now is mounted at the Nasmyth focus of UT3 where it had its first light in May 2014.

2. High contrast imaging

The main difficulties in observing a faint companion very close to the host star ($\leq 0.5 \text{ arcsecs}$) are the small angular distance between the two and the strong glare of the star with respect to the planet (contrast). The host star could be brighter by a factor of at least 10^5 that optical effects hinder or prevent the collection of photons directly from the target of observation. The first request could be realised enhancing the angular resolution of the instrument, for example using a large telescope ($D > 8 \text{ m}$) equipped with AO module that reshape the point spread function (PSF) very close to the diffraction figure. To tackle the second difficulty, it will be necessary to eliminate the diffraction peak using, for example, a coronagraph. At this point the only problem is the speckle noise that affects mainly the wings of the PSF. High-contrast imaging takes the requirements on PSF knowledge to extremes and has led to the instrumental and observational requirement that the complex speckle pattern in the wings of the PSF cancels out when data are combined. This requires very detailed char-

acterization of the PSF, which can be done under specific conditions. This could be done exploiting both instrumentation built on purpose of high contrast imaging and PSF reference technique optimised to eliminate or mitigate the speckle noise and PSF artefacts. In the following sections the technique used for SPHERE post reduction of data are described in some details.

2.1. Angular differential imaging

Angular differential imaging (ADI) is a high-contrast imaging technique that reduces quasi static speckle noise and facilitates the detection of nearby companions. Another name for this technique is roll deconvolution, a method that has previously applied with success on the HST images (Marois et al. 2006; Hinkley et al. 2007; Lafreniere et al. 2007; Artigau et al. 2008). The sensitivity of high-contrast ground-based AO imaging is limited primarily by quasi static speckle artifacts. If the wavefront sensing occurs in a plane that is different from the science focal plane, and if the speckles from the atmosphere and telescope pupil have been reduced in the wavefront sensing plane, there often remains a residual wavefront deformation in the science plane owing to a non-common-path problem. Especially at large separations ($> 0.5 \text{ arcsec}$), the main source of speckles is surface errors on the telescope primary mirror and internal optics. These speckles can be substantial, and since they arise from the telescope optics themselves, they can persist for a long time, typically many minutes or more. Unfortunately, a telescope speckle has the same appearance as an exoplanet, at a given wavelength, so strong, persistent speckles can easily overwhelm a faint exoplanet image. The angular differential imaging (ADI) technique can overcome internal speckles from the telescope (for alt/azimuthal telescopes) by simply allowing the FOV to rotate due to the Earth's rotation (except on the celestial equator). A sequence of images is acquired with an altitude/azimuth telescope while the instrument field derotator is switched off. This keeps the instrument and telescope optics aligned and allows the field of view to rotate with respect

to the instrument. Since the detector remains fixed with respect to the telescope, the non-common-path speckles also remain fixed on the detector. This setup improves the stability of the quasi static PSF structure throughout the sequence. On the contrary there is a slight rotation of the field of view (FOV), and only of it, with respect to the instrument. Once the raw images are reduced in the usual way (flat field, bad pixel subtraction and so on) if all the images are seen in sequence the low mass companion (if any) is seen to move azimuthally around its host star while the optical artefact and speckles are at rest. The FOV rotation during an exposure causes that the companion PSFs are smeared in the direction of the movement. This effect increases linearly with angular separation and slightly decreases companions peak intensity. Short exposures and the use of an optimized aperture photometry box can minimize this effect. For each image, after data reduction and image registration of the whole sequence, a reference PSF obtained from other images of the same sequence is subtracted to remove the quasi static structure. Given enough FOV rotation during the sequence, this subtraction preserves the signal from any eventual companion. All the image differences are then rotated to align the FOV and are median combined. Since the median is taken over a large number of images, the pixel-to-pixel noise (i.e., PSF, flat field, dark and sky Poisson noises, and detector readout noise) of the reference image is much less than that of any individual image (Marois et al. 2006). The ADI technique attenuates the PSF noise in two steps. First of all the subtraction of a reference image removes the correlated speckles. Secondary the combination of all residual images after FOV alignment allows to average the residual noise.

2.2. Spectral differential imaging

Among the several techniques that are able to reduce or remove the speckle noise there is the "spectral difference imager" (SDI) technique developed by different authors (Racine et al. 1999; Lenzen et al. 2004; Marois et al. 2005). The general principle of SDI is that two

images of the star acquired simultaneously at close wavelengths can be subtracted to remove most of the stellar halo and speckle pattern. In fact speckles are located at an angular distance from the star in proportion to their wavelength. If images are taken at wavelengths very close together, so the PSF is as similar as possible in the two images, and the two images are also taken simultaneously, in order to avoid that the speckle pattern will change from one to the next, and they are radially scaled to a common wavelength, then the difference of images should cause the fixed-pattern speckles to drop out. An additional leverage factor arises if the exoplanet has a strong absorption feature in its spectrum, different from its star. For example planetary spectrum has deep absorption features like the methane band at $1.7 \mu\text{m}$. The fact that the planet is relatively faint in this band gives it an extra possibility for detection (Racine et al. 1999; Marois et al. 2005; Biller et al. 2006). By taking simultaneous images in and out of the methane absorption band, and scaling and subtracting the two images, one effectively removes the residual starlight, while leaving the planetary light intact or almost intact. To ensure optimal rejection of the speckle noise, the images must be aligned, resampled on the same spatial scale, and scaled in intensity to account for any filter transmission and stellar flux variation. The method produces gains in dynamic range of about one or two magnitudes. SDI is, however, limited in application as it relies on an intrinsic feature of the companion spectrum; the CH_4 absorption feature only found in objects with $T_{\text{eff}} < 1200 \text{ K}$. In addition, there is a need for follow-up spectroscopy of the candidate object detected both to confirm its nature (often via common proper motion with the parent) and to characterize it in detail. Increasing the spectral resolution, initially suggested by Sparks & Ford (2002), can vastly increase the power of this technique, and it becomes a somewhat different speckle suppression method.

2.3. Spectral deconvolution

Several authors (e.g. Sparks & Ford 2002; Fusco et al. 2005; Berton et al. 2006) have sug-

gested that the wealth of spectral information available in an IFS data cube can be utilized to remove scattered starlight and identify the presence of a close-in companion, and extract its spectrum with enhanced SNR, thus maximizing contrast. The use of an IFS produces as output a data cube of images that has two of the three dimension that are spatial one and the third that is along the spectral dimension. Each image is a monochromatic representation of the scene that the instrument is observing. Each image of the data cube is affected by speckles and PSF artefacts. The speckle noise pattern is chromatic. Because the typical dimension of a speckle is about λ/D they will move radially in an image as a function of wavelength. In this type of data, the speckles follow diagonal paths through a data cube, while any genuine astrophysical structures have fixed positions with wavelength. This type of data also allows for extraction of spectra of the objects of interest with a resolution between 30 and 80. This technique does not rely on any feature of the target object's spectrum and is therefore applicable to any high-contrast imaging application. Spectral deconvolution (SD), this is the name of the technique, makes use of the fact that the position of almost all features arising from the parent star (Airy pattern, speckles, etc.) scales smoothly and slowly with wavelength (e.g. the first Airy null is always $1.22\lambda/D$ from the star), whereas a physical object's location is independent of wavelength. Thus, stepping through the wavelength axis of an IFS data cube at a fixed spatial location (e.g. the location of a companion), one would see a modulation arising from maxima and minima of the Airy pattern passing through the companion's location (Sparks & Ford 2002). These modulations would drown out any expected signal from the companion. If, however, we use the wavelength dependence to advantage, we can effectively subtract all wavelength-dependent artefacts in the stellar PSF, thus unmasking the presence of real physical objects. For a data cube obtained using IFS, spatially rescaling each individual slice proportionally to its wavelength aligns the speckles but makes the planet move inward with increasing wavelength. Speckles are now well fitted by a smooth (e.g., a low-order poly-

nomial) function to each pixel along the cube's dispersion axis while the planet produces a narrow bump while traveling through the pixel at a certain wavelength range. Because this bump is badly fitted by the smooth function, the subtraction of the fit removes most of the speckles and leaves the planet. This latter method has been used to reach 9 mag contrast at 0.2 arcsec separation without a coronagraph (Thatte et al. 2007). Here we list the most important steps needed to implement the SD. First, each monochromatic frame in the datacube is rescaled according to its wavelength in such a way that the speckle pattern is at least ideally the same while the position of an eventual companion is different from frame to frame tracing a diagonal line through the data cube. After that a fit is performed along the rescaled datacube wavelength direction for each pixel. The fitting function is then subtracted from the rescaled datacube. The degree of the fitting function can be selected in such a way to maximize the speckle noise subtraction and, in the meantime, to avoid subtracting signal from the companion. Finally, each frame is rescaled back to its original dimension so that the companion is always in the same position. At separation less than the bifurcation radius (Thatte et al. 2007) the spectrum is completely covered by an eventual companion that, for this reason, would be completely canceled so that the method is not effective at these small separations. The SD method can provide good results on SPHERE data as the instrument meet some particular characteristics: the speckles do scale linearly and the chromaticity of the speckles can be completely described by a low order polynomial. The SD technique holds great promise for direct imaging of exoplanets, as it simultaneously detects and spectrally characterizes any faint companion, thus removing the need for expensive and time-consuming follow-up observations, either to detect common proper motion or to obtain a spectrum of the faint companion. In addition, the technique does not require any assumptions about the companion's spectral characteristics (e.g. presence of a CH_4 feature), and can therefore be applied to any high-contrast application.

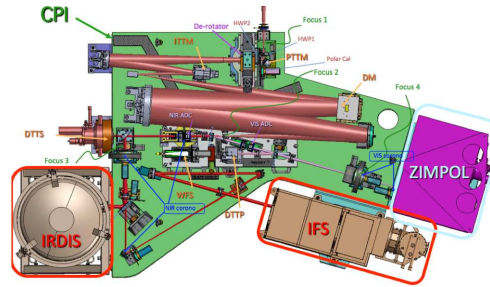


Fig. 1. SPHERE. In the sketch is possible to recognise the four main subsystems described into the text

3. SPHERE

The SPHERE planet-finder instrument installed at the VLT (Beuzit et al. 2008) is a highly specialized instrument dedicated to high-contrast imaging, built by a wide consortium of European laboratories. The Instrument is made of four subsystems (see Figure 1): the Common Path Optics and three science channels, a differential imaging camera (IRDIS), an Integral Field Spectrograph (IFS), and a visible imaging polarimeter (ZIMPOL). The Common Path includes pupil stabilizing fore optics (tip-tilt and derotator), the SAXO extreme adaptive optics system with a visible wavefront sensor, and NIR coronagraphic devices in order to feed IRDIS and IFS with highly stable coronagraphic images. Classical differential imagers and IFS are then clearly complementary in their properties, and an instrument where both these science modules are available may be extremely powerful for planet search. IFS explores the stellar neighborhood in order to find planetary spectral features. This quest is conducted searching for strong CH_4 absorption bands in both the stellar light reflected by gaseous Jupiter-like planets and in thermal emission from young-warm planets. Moreover it will be possible to have a first order characterization of the low mass companion itself. Additional science topics addressed by SPHERE include the study of protoplanetary discs, brown dwarfs, evolved massive stars and Solar System and extragalactic science. In the following a brief description of the main subsystems and scientific instrument is given. The AO module on board on SPHERE,

SAXO (Fusco et al. 2006; Petit et al. 2014; Sauvage et al. 2014), includes a 41×41 actuator high-order deformable mirror from CILAS with a maximum stroke $> \pm 3.5 \mu\text{m}$, and a 40×40 lenslet visible Shack–Hartmann wavefront sensor, based on the dedicated 240×240 pixel electron multiplying CCD220 from EEV achieving a temporal sampling frequency of 1.2 kHz with a read-out-noise < 1 electron and a 1.4 excess photon noise factor. The wavefront sensor is equipped with a focal plane spatial filter for aliasing control. At the heart of the AO system is the ESO standard real-time computer platform called SPARTA providing a global AO loop delay < 1 ms. SPARTA allows to control the system loops while also providing turbulent parameters and system performance estimation as well all the relevant data for an optimized PSF reconstruction and a clever signal extraction from scientific data. After the XAO module the light path goes towards the scientific instruments. After the splitting due to a NIR–Visible beam splitter, in the NIR part of the beam could be inserted several coronagraphic devices. The base-line coronagraph suite will include an achromatic four-quadrant phase mask coronagraph based on precision mounting of four half-wave plates, and both a classical Lyot coronagraph and an apodized Lyot coronagraph (Boccaletti et al. 2008). The NIR beam is then subdivided in two branches, one feeds IRDIS and the second part IFS. The IRDIS science module (Dohlen et al. 2008) covers a spectral range from $0.95 - 2.32 \mu\text{m}$ with an image scale of 12.25 mas consistent with Nyquist sampling at 950 nm. The FOV is $11 \times 12.5 \text{ arcsec}^2$, both for direct and dual imaging. Dual band imaging is the main mode of IRDIS, providing images in two neighboring spectral channels with < 10 nm rms differential aberrations. Two parallel images are projected onto the same $2k \times 2k$ detector with $18 \mu\text{m}$ square pixels, of which they occupy about half the available area. A series of filter couples is defined corresponding to different spectral features in modeled exoplanet spectra. The classical imaging mode allows high-resolution coronagraphic imaging of the circumstellar environment through broad-, medium-, and narrow-band filters throughout

the NIR bands including K_s . In addition to these modes, long-slit spectroscopy at resolving powers of 50 and 500 is provided, as well as a dual polarimetric imaging mode. A pupil-imaging mode for system diagnosis is also implemented. IFS is a very versatile instrument, well adapted for spectroscopic differential imaging as needed for detection of planets around nearby stars (Claudi et al. 2008, 2014). The main advantage of IFS is that differential aberrations can be kept at a very low level; this is true in particular for lenslet-based systems, where the optical paths of light of different wavelength within the IFS itself can be extremely close to each other. Additionally, IFS provide wide flexibility in the selection of the wavelength channels for differential imaging, and the possibility to perform spectral subtraction, which in principle allows recovering full information on the planet spectra, and not simply the residual of channel subtraction, as in classical differential imagers. The main drawback of IFS is that they require a large number of detector pixels, resulting in a limitation in the field of view, which is more severe for lenslet-based systems. Fed by the visible part of the optical beam, ZIMPOL is located behind the SPHERE visible coronagraph. Among its main specifications are a bandwidth of 600–900 nm and an instantaneous field of view of $3 \times 3 \text{ arcsec}^2$ with access to a total field of view of 8 arcsec in diameter by an internal field selector (Thalmann et al. 2008). The ZIMPOL optical train contains a common optical path that is split with the aid of a polarizing beamsplitter in two optical arms, each with its own detector. The common path contains common components for both arms like calibration components, filters, a rotatable half wave plate and a ferroelectric liquid crystal polarization modulator. The two arms have the ability to measure simultaneously the two complementary polarization states in the same or in distinct filters. The images on both ZIMPOL detectors are Nyquist sampled at 600 nm. The basic ZIMPOL principle for high-precision polarization measurements includes a fast polarization modulator with a modulation frequency in the kHz range, combined with an imaging photometer that demodulates the intensity sig-

nal in synchronism with the polarization modulation. The polarization modulator and the associated polarizer convert the degree of polarization signal into a fractional modulation of the intensity signal, which is measured in a demodulating detector system by a differential intensity measurement between the two modulator states. Each active pixel measures both the high and low states of the intensity modulation and dividing the differential signal by the average signal eliminates essentially all gain changes, notably changes of atmospheric transparency or electronic gain drifts.

4. First results

The first part of the commissioning of the instrument started on mid May 2014 and after the commissioning phase started the science verification phase. Various targets were observed to verify the capability of the instrument. The results obtained so far are very encouraging. Most of the targets observed are object of dedicated papers so we will not present them in this paper. Nonetheless, it is very interesting to show how SPHERE actually works and what beautiful results can obtain. We start with the white dwarf companion to HD114174 observed by SPHERE at a separation of 0.65 arcsec and a contrast of ~ 10.5 magnitudes with respect to the central star (see Figure 2). The companion was already observed with NIRC2 at Keck in 2012 (Crepp et al. 2013).

In the first run of commissioning also the star ι Sgr (HR7581, $J = 2.29$, K giant, $D = 55.7 \pm 0.6$ pc) has been observed. The star was previously known as an astrometric binary (Makarov et al. 2005) but the companion was never detected before. The IFS observing mode was Y-J. Once the IFS data cube was reduced with Spectra Deconvolution and ADI, the faint companion was clearly detected ($SNR = 50$) at an angular separation of $\theta = 0.249$ arcsec (see Figure 3) and a contrast of 9 mag. The object was simultaneously seen by IRDIS.

Using $\Delta m = 9$ mag the calibration by Delfosse et al. (2000), give a corresponding main sequence mass is $0.36 M_{\odot}$. From the IFS and IRDIS data it is also possible to get the spectrum of the faint companion (see Figure 4)

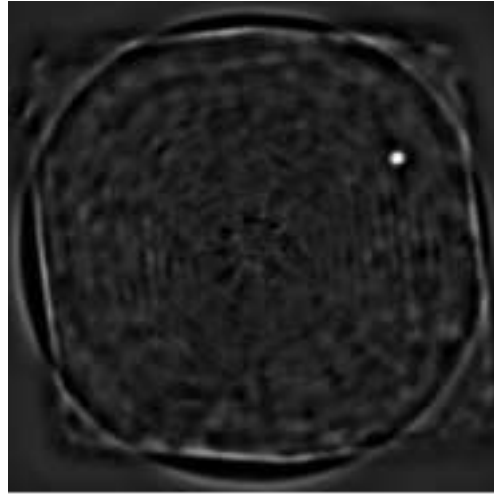


Fig. 2. Final image obtained for the star HD114174. The know WD companion is clearly visible on the top right corner while the central star, more than 10^4 times brighter, has been well cancelled using ADI and SD implemented in the SPHERE subtraction procedures.

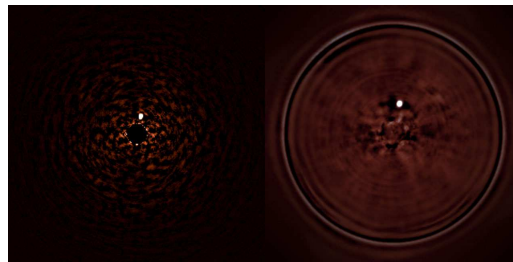


Fig. 3. The companion of ι Sgr is clearly visible in the images taken with both IFS and IRDIS. The central star is 4×10^3 times brighter than the M dwarf, but its image has been well cancelled by the subtraction procedures (<http://www.eso.org/public/news/eso1417/>).

that results to be essentially flat, as expected for an early M-type star on IFS spectra.

Figure 5 shows a collection of images obtained with SPHERE during the commissioning phase. The Jupiter's moon Io is imaged with some details of its surface. Titan (in the bottom of the picture) was observed by Zimpol. The disk of HR4796 is clearly visible while the glare of the central star is cancelled by SPHERE.

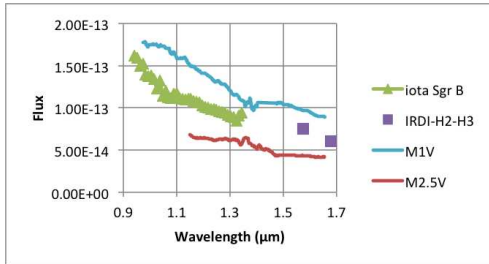


Fig. 4. The spectrum (in $W/m^2/\mu m$) of ι Sgr B as obtained by the IFS data (green triangles) and IRDIS (violet squares) compared with those of two M stars of different spectral types, scaled at the distance of this system.

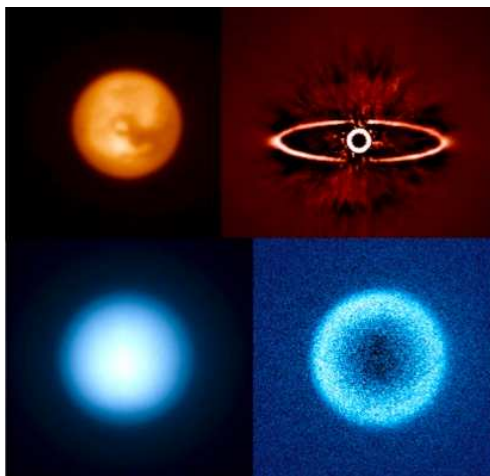


Fig. 5. Collection of several images obtained with the different science instruments of SPHERE

5. Conclusions

After about ten years of work, SPHERE finally is on duty at the UT3 of VLT. This new generation high contrast imager, together with its American competitor GPI will open a new era of very exciting discoveries not only in the field of extrasolar Planets. In fact they will give their contribution also in disk science and in the observation of the bodies of our Solar System.

References

Artigau, É, et al. 2008, Proc. SPIE, 7014, 70141Z
 Bailey, V., et al. 2014, ApJ, 780, L4

Berton, A., et al. 2006, PASP, 118, 1144
 Beuzit, J-L., et al. 2008, Proc. SPIE, 7014, 701418
 Biller, B. A., et al. 2006, Proc. SPIE, 6272, 62722D
 Biller, B., et al. 2012, ApJ, 753, L38
 Boccaletti, A., et al. 2008, Proc. SPIE, 7015, 70156E
 Bonnefoy, M., et al. 2014, A&A, 562, A111
 Brandt, T. D., et al. 2014, ApJ, 794, 159
 Brandt, T. D., et al. 2014a, ApJ, 786, 1
 Carson, J., et al. 2013, ApJ, 763, L32
 Claudi, R. U., et al. 2008, Proc. SPIE, 7014, 119
 Claudi, R., et al. 2014, Proc. SPIE, 9147, 91471L
 Close, L., et al. 2013, Into the Blue: AO Science in the Visible with MagAO, Proceedings of the Third AO4ELT Conference, Esposito, S., Fini, L. eds
 Close, L. M., et al. 2014, ApJ, 781, L30
 Crepp, J. R., et al. 2013, ApJ, 774, 1
 Delfosse, X., et al. 2000, A&A, 364, 217
 Dohlen, K., et al. 2008, Proc. SPIE, 7014, 126
 Esposito, S., et al. 2012 SPIE Conference Series, 8447
 Fusco, T., et al. 2005, Proc. SPIE, 5903, 593
 Fusco, T., et al. 2006, Optics Express, 14, 7515
 Galicher, R., et al. 2014, A&A, 565, L4
 Hinkley, S., et al. 2007, ApJ, 654, 633
 Hinkley, S., et al. 2013, ApJ, 779, 153
 Janson, M., et al. 2013, ApJ, 778, L4
 Kuzuhara, M., et al. 2013, ApJ, 774, 11
 Lafrenière, D., et al. 2007, ApJ, 660, 770
 Lagrange, A-M., et al. 2010, Science, 329, 57
 Lenzen, R., et al. 2004, Proc. SPIE, 5492, 970
 Macintosh, B., et al. 2014, Proceedings of the National Academy of Science, 111, 12661
 Makarov, V. V., et al. 2005, AJ, 129, 2420
 Males, J. R., et al. 2014, ApJ, 786, 32
 Marois, C., et al. 2005, PASP, 117, 745
 Marois, C., et al. 2006, ApJ, 641, 556
 Marois, C., et al. 2008, Science, 322, 1348
 Marois, C., et al. 2010, Nature, 468, 1080
 Meshkat, T., et al. 2013, ApJ, 775, L40
 Oppenheimer, B. R., et al. 2012, Proc. SPIE, 8447, 844720
 Oppenheimer, B. R., et al. 2013, ApJ, 768, 24
 Petit, C., et al. 2014, Proc. SPIE, 9148, 91480
 Racine, R., et al. 1999, PASP, 111, 587

- Rameau, J., et al. 2013, *ApJ*, 772, L15
Sauvage, M., et al. 2014, *Proc. SPIE*, 9143, 91431B
Skemer, A. J., et al. 2012, *ApJ*, 753, 14
Skemer, A., et al. 2014a, *IAU Symposium*, 299, 70
Skemer, A. J., et al. 2014b, *ApJ*, 792, 17
Skrutskie, M. F., et al. 2010, *Proc. SPIE*, 7735, 77353H
Sparks, W. B., & Ford, 2002, *ApJ*, 578, 543
Tamura, M., et al. 2010, in *In the Spirit of Lyot*
Thalmann, C., et al. 2008, *Proc. SPIE*, 7014, 120
Thatte, N., et al. 2007, *MNRAS*, 378, 1229